Magnetoacoustic geometric oscillations for longitudinal sound in beryllium*

E. F. Vozenilek[†] and Robert W. Reed

Department of Physics, The Pennsylvania State University, University Park, Pennsylvania 16802

(Received 17 March 1975)

Magnetoacoustic, geometric oscillations have been observed in the absorption of longitudinal ultrasound in single crystals of Be of high purity. The investigation was carried out at 1 K using sonic frequencies from 0.5 to 1.85 GHz. Caliper dimensions of the cigar and coronet pieces of the Fermi surface in Be were determined. These dimensions are consistent with the current theoretical models for the Fermi surface in Be.

INTRODUCTION

The Fermi surface (FS) of Be consists of a second-zone hole surface, called the "coronet," and third-zone electron surfaces called "cigars." Theoretical models[1-3] for the FS are consistent with experimentally derived data, most of which determined extremal cross-sectional areas of the FS.[1,4,5] Magnetoacoustic geometric oscillations in the ultrasonic attenuation yield caliper dimensions of the FS and thus provide a more specific test of a FS model than cross-sectional-area data of the de Haas–van Alphen (dHvA) type.

For observation of magnetoacoustic geometric oscillations it is necessary that (i) the electron mean free path l be large compared with the radius of the electronic cyclotron orbit, and (ii) $ql \gg 1$, where q is the sonic wave number. Our earliest investigations at sonic frequencies <0.5 GHz, using our best Be specimens, yielded only a few geometric oscillations. The range of frequencies over which we could work was extended to ~2 GHz by improving the apparatus (electronics and sample holder), and mastering the techniques for the vapor deposition of thin-film CdS transducers and for making indium acoustic bonds between the Be specimens and quartz delay rods.

MAGNETOACOUSTIC GEOMETRIC OSCILLATIONS: THEORY

Magnetoacoustic geometric oscillations in the ultrasonic attenuation in a metal at liquid-helium temperatures are observed when $\vec{q}$ and $\vec{B}$ (the magnetic induction in the specimen) are perpendicular to each other. Here Gaussian units are used and $\mu = B/H$ is taken as 1 G/Oe. The oscillations are periodic in $1/B$; their magnetic frequency F_G, in gauss, is related to a caliper Δk (a linear dimension in $\vec{k}$ space) of the FS by the equation[6,7]

$$\Delta k = \frac{e}{\hbar c} \frac{V_s}{f_s} F_G , \qquad (1)$$

where f_s and V_s are the sonic frequency and speed of propagation. This caliper Δk is measured in a direction perpendicular to $\vec{B}$ and to $\vec{q}$, and is an extremal (maximum or minimum) value, with respect to $\partial/\partial k_B$, of the calipers in the direction

$\vec{q} \times \vec{B}$ of cyclotron orbits in parallel planes separated from each other by dk_B.

In general the Δk caliper does not lie along a radius of a sheet of the FS. However, if the FS sheet has a plane of mirror symmetry perpendicular to $\vec{q}$ and a point of inversion symmetry in that plane, a radial Δk (extreme), for it, may give rise to magnetoacoustic geometric oscillations as described by Eq. (1).[8]

Equation (1) is derivable by integration of the Lorentz-force equation and scaling the diameters of the cyclotron orbits in real space in sonic wavelengths λ. Maxima in the attenuation oscillations appear when the real-space orbit diameter in the direction of $\vec{q}$ equals $(n + \phi_n)\lambda$, where n is an integer, and ϕ_n is a phase factor dependent on the orbit shape and on n. For a circular orbit,[9] $n + \phi_n = 1.22, 2.23, \ldots, (n + 0.25)$. For a rectangular orbit, $n + \phi_n \rightarrow n + 0.0$ as $n \rightarrow \infty$. Equation (1) assumes $\phi_{n+1} - \phi_n \sim 0$. No contradiction of this assumption was observed in any of the data (for the values of n actually used in the data analysis) of this investigation.

Mathematical theories for magnetoacoustic geometric oscillations are included in Refs. 6, 7, and 10–12. Mertsching[7] has given the following formula for the oscillatory component $\alpha_L(\text{osc})$ of the attenuation coefficient for longitudinal sound in the limit $ql \gg 1$:

$$\alpha_L(\text{osc}) = G \left[\left(\frac{2\pi}{q |\partial^2 D/\partial k_B^2|} \right)^{1/2} \right.$$

$$\left. \times \frac{m_c \Lambda_L^2}{|\partial v_l/\partial \theta|} \frac{\cos(qD - \frac{3}{4}\pi)}{\sinh(\pi/\omega_c \tau)} \right]_{\vec{q} \cdot \vec{v}_F = 0} , \qquad (2)$$

$$D = \text{max, min}$$

where

$$G = \omega_s / 2\pi^2 \hbar^2 V_s^2 \rho .$$

Λ_L is the deformation potential for the FS deformed by longitudinal sound, τ is the electronic scattering time, $\omega_c = |e| B / m_c c$, ω_s is the angular sonic frequency, ρ is the mass density of the crystal, $v_l = \vec{v}_F \cdot \hat{q}$, and θ is the polar angle in the plane of the cyclotron orbit. The factors Λ_L, $|\partial^2 D/\partial k_B^2|$, and

$|\partial v_l/\partial \theta|$ are the FS properties that influence the amplitude of the magnetoacoustic oscillations. As the zero-field attenuation is proportional to Λ_L^2, the amplitude of the magnetoacoustic oscillations is proportional to the zero-field attenuation. D is the caliper of the cyclotron orbit along $\vec{q}$ in real space, but $|\partial^2 D/\partial k_B^2|_{D\,(\text{extreme})}$ is proportional to the curvature, in the plane perpendicular to $\vec{q}$, of the FS in $\vec{k}$ space at $\vec{k}_F \| \hat{q} \times \hat{B}$. The real space dimension D is related to the corresponding $\vec{k}$-space dimension Δk by $D = c\hbar\Delta k/|e|B$. When $\partial^2 D/\partial k_B^2$ is small, many cyclotron orbits contribute in phase to $\alpha_L(\text{osc})$. The factor $\partial v_l/\partial \theta$ is to be evaluated where $v_l = \vec{v}_F \cdot \hat{q} = 0$, i.e., where the electron travels parallel to the sonic wave front and the probability of sonic phonon-electron interaction is largest. The smaller $|\partial v_l/\partial \theta|_{v_l=0}$ is, the longer is the duration of this interaction and the larger the resulting value of $\alpha_L(\text{osc})$.

THE FERMI SURFACE OF BERYLLIUM

Be crystallizes in the hcp structure with a c/a ratio of 1.5689. The FS of Be has been the subject of several theoretical calculations including orthogonalized-plane-wave (OPW) calculations by Loucks and Cutler[2] and Loucks[3] and an augmented-plane-wave (APW) calculation by Terrell.[13] These calculations yielded a FS that deviated substantially from the free-electron model of Harrison.[14] The semiempirical, nonlocal pseudopotential calculations by Tripp, Everett, Gordon, and Stark (TEGS)[1] give the best fit to the body of experimental FS data available at present. In the TEGS calculation the pseudopotential parameters were adjusted to yield agreement with their experimental dHvA data.

The first Brillouin zone is shown in Fig. 1 along
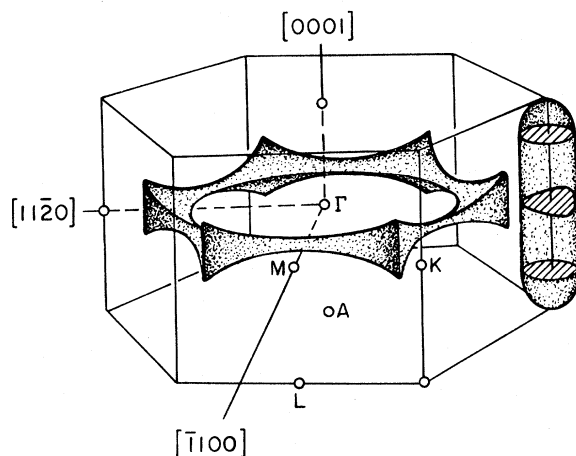
FIG. 1. First Brillouin zone and Fermi surface for Be. The "coronet" is an electron-hole surface in the second Brillouin zone, and the "cigars" are electron surfaces in the third Brillouin zone.

with the Be model Fermi surface. The FS of Be consists of a second-zone hole surface called the "coronet" and six equivalent third-zone electron surfaces which can be combined to form two "cigars" per coronet.

In the basal plane the coronet is continuous with six lobes at 60° intervals around the c axis, [0001] direction. The vertices of the lobes are on the equivalent $\langle 11\bar{2}0 \rangle$ directions, and the lobes are joined by narrow necks, which are smallest in cross section in the equivalent $\langle 10\bar{1}0 \rangle$ directions.

The cigar is roughly triangular in cross section at its mid-section, which lies in the basal plane with a vertex of the triangle adjacent to a lobe of the coronet. The cigar and the coronet are separated by a small energy gap.

The mid-cross-section of the cigar in the ΓKM plane, called the "waist," has a 3% smaller area than the cross sections displaced up or down by a third of the distance KH. The larger areas are called the "hips" and are believed to be more nearly circular in cross section.[2]

EXPERIMENTAL METHODS AND PROCEDURES

The ultrasonic attenuation measurements were made as a function of the magnetic field intensity H at frequencies from 0.5 to 1.85 GHz. The pulse-echo method was used with a double-ended (i.e., separate driver and receiver) transducer configuration. The ultrasonic apparatus, which includes automatic gain control of the receiving amplifiers and synchronous detection of a selected sonic echo for improved signal to noise and high stability, has been described in detail elsewhere.[15,16] The ultrasonic frequencies were determined to within ± 0.5 MHz with a calibrated cavity wave meter for frequencies below 1.2 GHz. For frequencies above 1.2 GHz, the frequency was determined to within ± 3 MHz using a calibrated local oscillator.

Three Be specimens, in the form of disks ~ 9.5 mm in diameter and ~ 2 mm thick with axes along the [0001], [10$\bar{1}$0], and [11$\bar{2}$0] crystalline directions, were supplied by Mr. Jack Conner of the Reactor Development and Technology Division of the U.S. Atomic Energy Commission and were grown by Nuclear Metals Inc. The specimens were machined by spark erosion. CdS transducers ~ 2 μm thick (for longitudinal sound) were vapor-deposited on one face of each specimen. On the other face a thin film of In was vapor-deposited. A thin film of In was also deposited on one face of a Z-cut quartz delay rod, 1.0 cm long by 0.953 cm in diameter. An acoustic bond was formed by pressing the In-coated end of the delay rod and the Be specimen together at a temperature of 150 °C for 12 h so that the In films fused together. The free end of the delay rod was coated with an Al electrode onto which a CdS transducer was evaporated.

The sonic specimens were mounted in a rotatable sample holder,[17] placed in a finger Dewar which was mounted inside the bore of a superconducting solenoid. $\vec{q}$ was aligned along the axis of rotation which was in turn perpendicular to $\vec{H}$ within $\pm 0.5°$. Using a worm gear drive connected to a 30-turn counting dial outside the cryostat, the orientation of a specimen axis with respect to $\vec{H}$ (vertical) could be determined with a repeatability of $\pm 0.2°$. Measurements on the specimens were made at temperatures from 1.0 to 1.2 K.

Two superconducting solenoids made by American Magnetics, Inc. of Oak Ridge, Tenn. were used. A small solenoid for fields up to 10 kOe in a 6.4-cm bore had a uniformity of 1 in 10^4 over a 2-cm length along the coil axis and an inductance of only 0.45 H. The small inductance made it useful for field modulation at frequencies up to 10 Hz. The power supply for this solenoid was a Kepco Bipolar Operational Power Supply model BOP-15M-20. This supply was programed to supply a slowly varying current I ($dI^{-1}/dt = $ const.) on which was superimposed a modulating current with amplitude proportional to I^2. Since $H \propto I$, this resulted in the amplitude ΔH of the field modulation remaining the same fraction of a magnetoacoustic period for all values of H.

The second superconducting solenoid was rated for fields to 75 kOe in a bore of 10.2 cm. This solenoid had a uniformity of field of 1 in 10^4 over a 2-cm-diameter spherical volume about the sample. A Didcot Instrument Co., Ltd., model DPS A/100/4.5/1 constant-current power supply, with a stability of better than 1 in 10^4, powered the large solenoid. It was programed to deliver a current ($dI^{-1}/dt = $ const.) by a modified Varian, model X-4115 superconducting magnet, $1/H$ sweep unit.

The small superconducting solenoid could be mounted inside the bore of the large solenoid to provide a modulating field in addition to the high field of the large solenoid. This large solenoid was necessary since geometric oscillations were observable at fields above 20 kOe for sonic frequencies of 1.85 GHz.

Both solenoids were wound with multifilament NbTi wire with the result that H was accurately linear with I. The H-vs-I calibrations of the solenoid were made using proton NMR measurements to determine H, and a $5\frac{1}{2}$-place digital voltmeter (with BCD output) to measure the voltage developed across a 10-mΩ standard resistor for the determination of I. H-vs-I calibrations were reliable to better than 0.1% for fields larger than 100 Oe.

Sonic attenuation vs magnetic field data were recorded with an X-Y recorder. The data were also punched simultaneously on paper tape for computer processing by the method of fast Fourier analysis. The punched data consisted of simul-

taneously measured values of echo-height voltage (to three places) and magnet current (to five places). Either 512 or 1024 data pairs were recorded for $1/H$ sweep ratios, $H_{max}:H_{min}$, of 10:1 and sweep times of 5–50 min. The solenoid-current axis on the X-Y recorder charts was calibrated at the beginning and end of each field sweep, so that data reduction could be accomplished by hand if the number of magnetoacoustic oscillations in α_L was too small for good computer analysis.

EXPERIMENTAL RESULTS

The various calipers that were obtained for the FS of Be were calculated from the observed period, $(1/B_{n+1} - 1/B_n) = F_G^{-1}$, of the magnetoacoustic oscillations in α_L using Eq. (1). The sound velocity V_s was calculated using the adiabatic elastic moduli for Be at 4.2 K given by Testardi and Condon,[18] who estimated the moduli to be accurate to 0.1%. The calculated velocities for the three principal directions are $V_s[0001] = 13.61 \times 10^5$ cm/sec and $V_s[11\bar{2}0] = V_s[10\bar{1}0] = 12.42 \times 10^5$ cm/sec.

$\vec{q}$ parallel to $[11\bar{2}0]$

Figure 2 is typical of echo-height-vs-H plots for $\vec{q} \parallel [11\bar{2}0]$ and $\vec{H} \parallel [0001]$. For Fig. 2, f_s was 1.850 ± 0.003 GHz and T was 1.2 K. Figure 2 was recorded on an X-Y recorder; when recorded on an expanded scale on a strip-chart recorder, as many as 38 oscillations were clearly visible. The superconducting-to-normal transition of the In acoustic bond is responsible for the sharp drop in echo height at ~ 250 Oe.

Figure 3 is an echo-height derivative vs $1/H$ plot, over a 10-to-1 range of H, of a portion of Fig. 2. In this case the magnetic field was modulated, and the echo height was synchronously detected with a lock-in amplifier operating at the
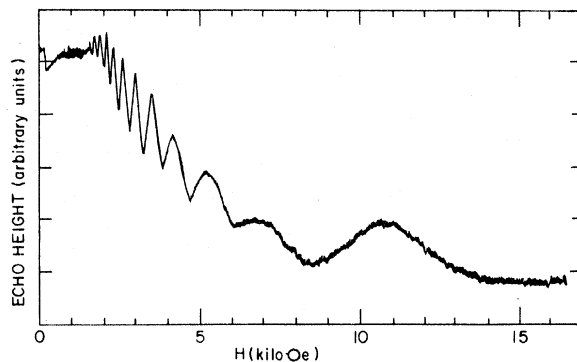
FIG. 2. Magnetoacoustic geometric oscillations for $\vec{q} \parallel (11\bar{2}0)$, $\vec{H} \parallel [0001]$, and sonic frequency 1.850 GHz. The abscissa scale is linear in H. The $n=1$ peak (a minimum in echo-height) is off the graph to the right at about 22 kOe.
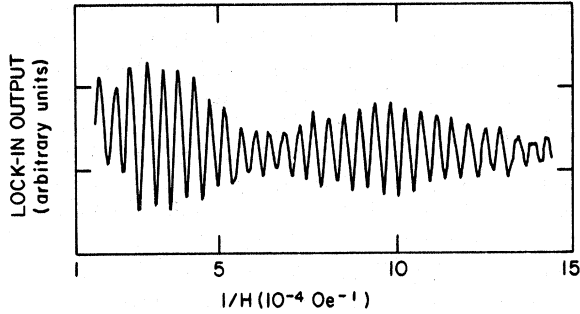
FIG. 3. Magnetoacoustic geometric oscillations. These oscillations are the H-field derivative of a portion of those in Fig. 2. The abscissa scale is linear in $1/H$.

modulation frequency. Hence the derivative of the Fig. 2 plot is recorded in Fig. 3. The method of field modulation with synchronous detection emphasizes the oscillations in α_L and rejects the background change.

All the oscillations seen in Fig. 2 could not be fitted in the range of the available 10 : 1 $1/H$ sweep. However, the advantages of the use of the $1/H$ sweep outweighed the loss of the oscillations. The data were fast-Fourier-analyzed, and the two periods contributing to the beats seen in Fig. 3 were determined. The Δk calipers that result are summarized in Table I for a number of sonic frequencies and angles between $\vec{H}$ and the [0001] axis. Using 1.040-GHz sound, fewer oscillations were observed and only one value of F_G was determined. No magnetoacoustic oscillations were observed when the angle between $\vec{H}$ and the [0001] axis exceeded 1°. For all the data used in the calculation of the values of F_G and Δk given in Table I, n (the serial number of the oscillations, starting at the high field end) exceeded 7.

TABLE I. Experimental caliper dimensions for $\vec{q} \parallel [11\bar{2}0]$. (1 a.u. is equal to the Bohr radius of the hydrogen atom.)

Sonic frequency (MHz ± 3 MHz)	Angle between H and [0001] (deg)	Magnetic frequency F_G (10^4 G)	Calipered dimension Δk (a.u.)$^{-1}$
1040	0	1.19 ± 0.04	1.14 ± 0.04
1850	0	2.09 ± 0.03	1.13 ± 0.02
		2.24 ± 0.04	1.21 ± 0.02
1850	0	2.06 ± 0.04	1.11 ± 0.02
		2.22 ± 0.02	1.20 ± 0.01
1850	0	2.10 ± 0.04	1.13 ± 0.02
		2.22 ± 0.02	1.20 ± 0.01
1850	0.4	2.10 ± 0.04	1.13 ± 0.02
		2.23 ± 0.04	1.20 ± 0.02
1850	0.8	2.10 ± 0.02	1.13 ± 0.01

The small angle (~1°) between $\vec{H}$ and the [0001] direction over which the data of Table I were observed, along with a comparison of the resulting Δk calipers with dimensions of the FS calculated by TEGS,[1] show that these calipers are for the inner and outer diameters of the coronet along the $M\Gamma N$ (or $\hat{q} \times \vec{H}$) direction. The TEGS values for the inner and outer diameters of the cornet along the $M\Gamma N$ axis are respectively 1.159 and 1.198 (a.u.)$^{-1}$. Using the theoretical TEGS values for the dimensions of the neck (distance on in Fig. 4), the calculated value for the critical tilt angle of $\vec{H}$ from the [0001] axis for observation of magnetoacoustic oscillations is 0.92°, which is in good agreement with our observations. The approach of the inner and outer calipers at the neck to a single value at the critical tilt angle is to be expected, as we observed at ~0.8°.

No other oscillations were observed for any other orientation of $\vec{H}$ for $\vec{q}$ directed along the [11$\bar{2}$0] axis.

$\vec{q}$ parallel to [10$\bar{1}$0]

When $\vec{q}$ was parallel to the [10$\bar{1}$0] axis (which is equivalent to the [$\bar{1}$100] axis of Fig. 1) and $\vec{H}$ was rotated in the (10$\bar{1}$0) plane, two different series of oscillations were observed. The higher frequency F_G oscillations were observed only when $\vec{H}$ was within 1° of the [0001] axis, see Fig. 5. A low-frequency bandpass filter was used with a $1/H$ sweep to separate the two series of oscillations. The data recorded in Fig. 5, for a sonic frequency of 1.501 GHz, were hand-calculated from calibrated X-Y charts that were linear in $1/H$. The major sources of uncertainty in the calculated Δk calipers arose from the uncertainty in the location in $1/H$ of the absorption maxima and from the small number of oscillations observed. The number of oscillations was too small for useful Fourier analysis.

The small Δk data near the [0001] axis in Fig. 5 were derived from a series of about ten oscillations. The number of observable oscillations decreased as the angle between H and the [0001] axis was increased until at ~60° the oscillations disappeared into the noise. The decreasing number and amplitude of the oscillations explain the longer
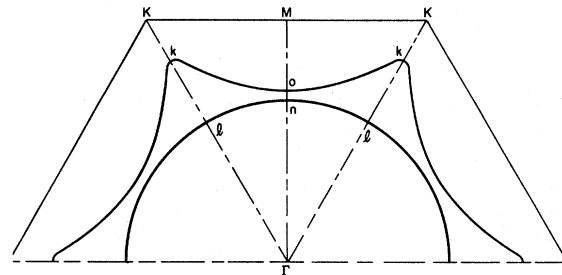
FIG. 4. Cross section of the coronet in the basal plane.
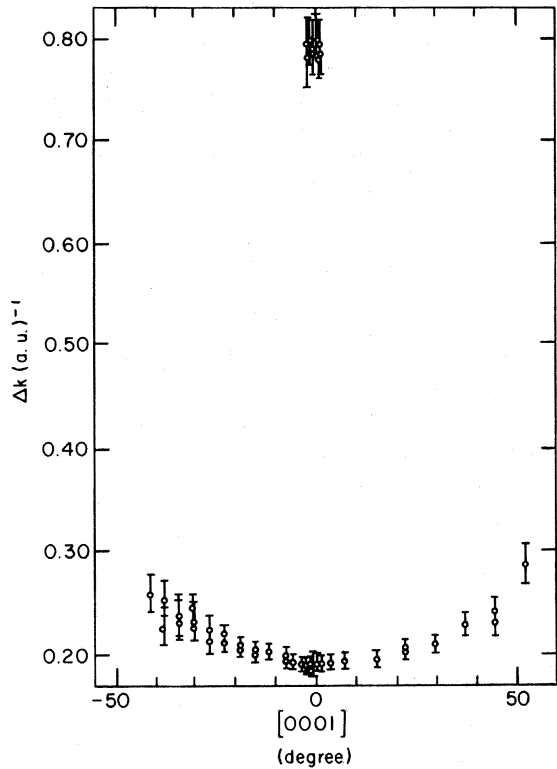
FIG. 5. Plot of observed Δk's for $\vec{q} \parallel [10\bar{1}0]$. The data are plotted as a function of the location of $\vec{H}$ from the [0001] axis in the $(10\bar{1}0)$ plane. The Δk calipers lie in $(10\bar{1}0)$ planes through the Fermi surface; e.g., Δk for $\vec{H} \parallel [0001]$ is along the $[11\bar{2}0]$ direction.

error bars in Fig. 5 at the larger angles.

The low Δk data in Fig. 5 are attributed to calipers of the cigar in the $(10\bar{1}0)$ plane, either at the waist or the hips. For $\vec{H}$ along the [0001] axis, $\Delta k = 0.193 \pm 0.004$ (a.u.)$^{-1}$ equal to $Ka + Kb$ in Fig.

6 for the waist or $rc + rd$ for the hips. The values for these dimensions are given by TEGS as 0.203 and 0.197 (a.u.)$^{-1}$, respectively. It is known from dHvA data that the cross-sectional area of the hips is larger than that of the waist. This does not preclude the possibility of a single extremal caliper for the cigar in the $(10\bar{1}0)$ plane. (The calipers given by TEGS have the waist slightly larger than the hips in this plane.) The very long section of the cigar having nearly the same extremal Δk in the $(10\bar{1}0)$ plane would be expected to give rise to large amplitude oscillations.

The Δk caliper for the oscillation with high F_G in Fig. 5 is constant, 0.804 ± 0.01 (a.u.)$^{-1}$ within experimental error, over an angle of $\pm 1°$ between $\vec{H}$ and the [0001] axis in the $(10\bar{1}0)$ plane, and is unobservable for larger angles. The smallness of the angle over which it is observed suggests that this Δk is some caliper of the coronet in the (0001) plane. Comparison with the coronet dimensions given by TEGS makes the kk caliper across adjacent wing tips in Fig. 4 appear to be a plausible source of the oscillations. The hexagonal symmetry makes $kk = \Gamma k = \Gamma l + lk$. Using the TEGS dimensions, the calculated value for Γk is 0.8295 (a.u.)$^{-1}$.

The failure to observe magnetoacoustic oscillations for an orbit around the inside of the cornet in the (0001) plane is not explained. Because a large number of oscillations from this orbit were observed (Fig. 2) for $\vec{q} \parallel [11\bar{2}0]$, one expects a similar result for $\vec{q} \parallel [10\bar{1}0]$. Since the caliper $\Delta k = 0.804$ (a.u.)$^{-1}$ was observed for $\vec{q} \parallel [10\bar{1}0]$, misorientation of the specimen is ruled out as an explanation.

$\vec{q}$ parallel to [0001]

The Be specimen used for this set of measurements with $\vec{H}$ in the (0001) plane and $\vec{q}$ along the
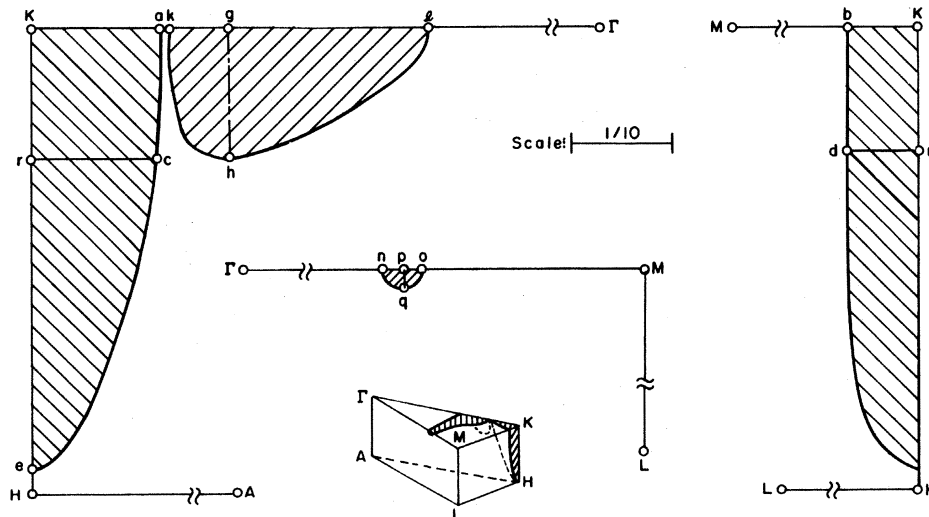
FIG. 6. Cross sections of the Be Fermi surface in various planes through the Brillouin zone. This figure is reproduced with permission from Loucks and Cutler (Ref. 2).
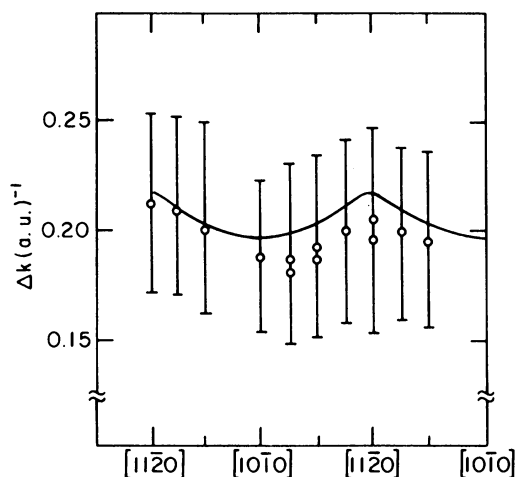
FIG. 7. Plot of Δk for $\vec{q} \parallel [0001]$. The data are plotted as a function of the location of $\vec{H}$ in the (0001) plane. The Δk calipers therefore lie in the (0001) plane.

[0001] axis appeared to be of poorer quality than the other two specimens. The oscillatory attenuation showed the dependence on sonic frequency expected from Eqs. (1) and (2), but only five oscillations were observed at the highest sonic frequency possible (1.42 GHz) with this specimen. With so few oscillations, neither analog filtering nor field modulation proved to be of more than marginal value. The Δk caliper obtained is consistent with calipers of the cigar in the (0001) plane. They are plotted in Fig. 7. The large error bars arise from the small number and amplitude of the $\Delta(1/H)$ periods observed. It is, however, observed that the value of 0.193 (a.u.)$^{-1}$ for $\vec{H} \parallel [0001]$ in Fig. 5 is

in good agreement with the value for the same caliper (parallel to $[11\bar{2}0]$) for $\vec{H} \parallel [10\bar{1}0]$ in Fig. 7. The difference in these two measures of the same caliper is much less than the error bars of Fig. 7. The error bars represent our maximum estimate of all possible uncertainties in the determination of the $\Delta(1/H)$ period.

The solid-line curve in Fig. 7 represents the dependence of the $Ka+Kb$ caliper in Fig. 6 to be expected for a cigar with triangular cross section as calculated by Loucks and Cutler[2] but normalized to 0.197 (a.u.)$^{-1}$ as predicted by TEGS for $\vec{H} \parallel [10\bar{1}0]$ in Fig. 7. The experimental data are in agreement with the theoretical curve.

CONCLUSIONS

Magnetoacoustic geometric oscillations have been observed at sonic frequencies up to 1.85 GHz. Caliper dimensions of both the cigar and the coronet sections of the Fermi surface of Be have been derived from this data. The absence of magnetoacoustic geometric oscillations for certain calipers of the Fermi surface is unexplained, since strong oscillations from closely related calipers were observed. The semiempirical pseudopotential model of the Fermi surface of Be by TEGS[1] is in very good agreement with our experimental data.

*Supported by the Applied Research Laboratory of the Pennsylvania State University, under contract with the U. S. Naval Sea Systems Command.

†Present address: Corning Glass Works, Sullivan Park, Corning, N. Y. 14870.

[1] J. H. Tripp, P. M. Everett, W. L. Gordon, and R. W. Stark, Phys. Rev. 180, 669 (1969).

[2] T. L. Loucks and P. H. Cutler, Phys. Rev. 133, A819 (1964).

[3] T. L. Loucks, Phys. Rev. 134, A1618 (1964).

[4] J. H. Condon, Phys. Rev. 145, 526 (1966).

[5] W. A. Reed and J. H. Condon, Phys. Rev. B 1, 3504 (1970).

[6] A. B. Pippard, Proc. R. Soc. A 257, 165 (1960).

[7] J. Mertsching, Phys. Status Solidi 37, 465 (1970).

[8] J. B. Ketterson and R. W. Stark, Phys. Rev. 156, 748 (1967).

[9] J. M. Ziman, Principles of the Theory of Solids (Cambridge U. P., London, 1964).

[10] M. H. Cohen, M. J. Harrison and W. A. Harrison, Phys. Rev. 117, 937 (1960).

[11] P. R. Sievert, Phys. Rev. 161, 637 (1967).

[12] M. P. Greene, A. R. Hoffman, A. Houghton, and J. J. Quinn, Phys. Rev. 156, 798 (1967).

[13] J. H. Terrell, Phys. Rev. 149, 526 (1966).

[14] W. A. Harrison, Phys. Rev. 118, 1190 (1960).

[15] R. W. Reed, D. E. Binnie, and F. G. Brickwedde, J. Acoust. Soc. Am. 51, 910 (1972).

[16] R. W. Reed, J. Acoust. Soc. Am. 56, 886 (1974).

[17] E. F. Vozenilek, Ph.D. thesis (The Pennsylvania State University, 1975) (unpublished).

[18] L. R. Testardi and J. H. Condon, Phys. Rev. B 1, 3928 (1970).